frontiers | Frontiers in Earth Science

TYPE Original Research
PUBLISHED 19 May 2025
DOI 10.3389/feart.2025.1588481

Multi-sphere coupling characteristics and gas-bearing controlling factors of calcareous shale reservoirs in the Yadu-Ziyun-Luodian Aulacogen under Early Carboniferous platform-basin transitional sedimentary system, South China

Kun Yuan[1,2,3], Bing Feng[4], Gangquan Li[4]*, Zongan Xue[1,2,3], Tuo Lin[1,2,3], Xinxin Fang[5]*, Xiangcan Sun[1,2,3]*, Yinbo Xu[1,2,3] and Fengzan Zheng[6]

[1]Oil and Gas Resources Survey, China Geological Survey, Beijing, China, [2]The Key Laboratory of Unconventional Oil and Gas Geology, China Geological Survey, Beijing, China, [3]State Key Laboratory of Continental Shale Oil, Beijing, China, [4]Guizhou Shale Gas Exploration and Development Co., Ltd., Zunyi, China, [5]Institute of Geomechanics, Chinese Academy of Geological Sciences, Beijing, China, [6]School of Energy Resources, China University of Geosciences, Beijing, China

The Early Carboniferous Dawuba Formation within the Yadu-Ziyun-Luodian aulacogen (YZLA), southern China, represents a significant shale gas play formed within a dynamic platform-basin transitional sedimentary system influenced by multi-sphere coupling (the dynamic interaction of tectonic, climatic, and oceanic spheres). This setting generated pronounced heterogeneities in lithology and gas content. Integrating field geological surveys and well data, this study comprehensively evaluates the mineralogy, geochemistry, structural features, and gas content of these shales to decipher the key factors controlling gas enrichment, particularly in this tectonically complex area. A crucial finding is the distinction between low-energy, "thick-bedded" deposits and higher-energy, "thin interbedded" sections characterized by frequent alternations of mudstone and argillaceous limestone (0.5–5 m single layers, mudstone:limestone ratio 1:1–1:2). Significantly, these thin interbedded sections demonstrate superior reservoir quality, exhibiting higher porosity (~2.9%) and notably higher gas content (~2.5 m^3/t). We reveal that in the YZLA's complex structural setting, shale gas content is primarily governed by preservation conditions dictated by the unique litho-mechanical properties of the interbedded strata, rather than traditional controlling factors like TOC abundance or matrix porosity. The frequent interlayering promotes stable micro-fractures, supported by clay-rich horizons and effectively sealed by compact limestone, thereby enhancing secondary storage capacity and permeability for free gas. Consequently, these thin interbedded sections represent the most favorable intervals for shale gas accumulation, identifying them as the

Check for updates

OPEN ACCESS

EDITED BY
Ahmed Reda,
Curtin University, Australia

REVIEWED BY
Rui Liu,
Southwest Petroleum University, China
Lingling Han,
University of Chinese Academy of Sciences, China
Ruiliang Guo,
Xi'an Shiyou University, China

*CORRESPONDENCE
Gangquan Li,
ctnyktkf@163.com
Xinxin Fang,
freestarxin@163.com
Xiangcan Sun,
sunxiangcan@mail.cgs.gov.cn

RECEIVED 06 March 2025
ACCEPTED 25 April 2025
PUBLISHED 19 May 2025

CITATION
Yuan K, Feng B, Li G, Xue Z, Lin T, Fang X, Sun X, Xu Y and Zheng F (2025) Multi-sphere coupling characteristics and gas-bearing controlling factors of calcareous shale reservoirs in the Yadu-Ziyun-Luodian Aulacogen under Early Carboniferous platform-basin transitional sedimentary system, South China.
Front. Earth Sci. 13:1588481.
doi: 10.3389/feart.2025.1588481

prime targets for achieving Early Carboniferous shale gas breakthroughs in the YZLA.

KEYWORDS

Southern China, Carboniferous, shale gas, lithologic interbedding, preservation conditions, gas content, aulacogen

1 Introduction

Shale gas has emerged as a significant global energy resource, fundamentally altering energy landscapes with successful exploitation in numerous basins worldwide (Alsaifet al., 2024). However, realizing the full potential of shale gas accumulations, particularly in mature or structurally complex basins, hinges critically on understanding and evaluating gas preservation conditions (Khan et al., 2024). While China has achieved notable success in relatively stable marine shale plays like the Lower Paleozoic Wufeng-Longmaxi Formation in the Sichuan Basin (Ma et al., 2017; Zou et al., 2019), exploration efforts in other prospective intervals, such as the widespread Carboniferous strata in southern China, are still developing and face unique challenges (Liu et al., 2017).

The Early Carboniferous Dawuba Formation within the Yadu-Ziyun-Luodian aulacogen (YZLA) in Guizhou Province, southern China, represents one such challenging Frontier. This region holds substantial estimated shale gas resources (~20.1 trillion m^3, approx. 28% of Guizhou's total) and has shown promising gas indications in recent exploratory wells (QSD1, QZY1) (Hao et al., 2013). However, the YZLA is characterized by significant geological complexities that directly impact exploration risk. The region underwent multiple phases of tectonic activity, resulting in extensive faulting, folding, and overall structural deformation (Arthur and Sageman, 1994; Li et al., 2015).

This complex tectonic history is a primary concern for shale gas preservation, as deformation can compromise seal integrity, reactivate faults creating leakage pathways, alter *in-situ* stress states affecting fracture permeability, and potentially lead to significant gas loss over geological time (Chen et al., 2020; Ma et al., 2022a). Compounding this structural complexity, the Dawuba Formation was deposited within a dynamic platform-basin transitional environment, leading to rapid vertical and lateral lithological variations, primarily involving thin interbedding of mudshales and argillaceous limestones (Chen et al., 2025).

Globally, assessing shale gas preservation involves evaluating a complex interplay of factors. Key considerations include the integrity and sealing capacity of regional caprocks, the distribution and sealing potential of faults, subsurface pressure and temperature regimes, the chemistry of formation waters, and present-day stress states (Li et al., 2022a; Mcmahon et al., 2024). Recent international research further emphasizes the importance of understanding pore structure evolution throughout burial history; initially, primary pores can be occluded by bitumen, but secondary porosity often develops with increasing thermal maturity, impacting storage and connectivity. Stable structural conditions are generally favorable for pore preservation, while compression can alter pore geometry and increase microfractures. Burial depth typically reduces porosity, although formation overpressure can help preserve it. Novel assessment techniques are also emerging, such as using carbon isotope fractionation (CIF) models combined with logging data, or rapid screening *via* Pyrolysis-FTIR to analyze gas composition and quantity (Mansour et al., 2024; Li et al., 2025). Research in China, particularly focused on complex geological settings like the Sichuan Basin (e.g., Longmaxi, Wujiaping, Longtan, Niutitang formations), Guizhong Basin, and Qiannan Basin, has similarly employed a range of indicators. These include traditional metrics like stratum dip, magnitude of erosion, variations in measured gas content (which can range significantly, e.g., 0.13–4.19 m^3/t in Niutitang shale or averaging 5.0 m^3/t in Longtan shale), alongside geochemical parameters such as TOC content, kerogen type, and thermal maturity (Ro) (Wang et al., 2021; Martyushev et al., 2023). Studies highlight that differences in preservation conditions, strongly influenced by structural deformation intensity, fracture development, and the coupling between depositional setting (e.g., deepwater shelf) and tectonics, are critical factors controlling gas content variations, especially in deep and ultra-deep shale plays (Rezaeyan et al., 2023). The preservation potential is often linked to specific structural styles, with low-angle monoclines and broad anticlines considered more fa vorable in some regions like Nanchuan, while tightly folded or faulted structures pose greater risks (Valdon et al., 2023).

Despite these advancements, a critical knowledge gap persists, both globally and within China, in fully understanding how specific depositional architectures (e.g., facies variations, initial fabric) interact with complex, multi-stage tectonic overprints to ultimately control gas retention and distribution. This is particularly challenging in regions that have experienced significant deformation post-deposition, such as parts of the Sichuan Basin or other complex tectonic zones (Greve et al., 2024; Zou et al., 2018). Tectonic activity through different phases critically influences sealing conditions and can lead to gas escape (Mcmahon et al., 2024). Many existing assessment methods, including the comprehensive "six-property" assessments (organic matter, lithofacies, petrophysics, gas content, brittleness, stress field), focus on identifying present-day leakage risks or characterizing reservoir quality ("sweet spots") (Sageman et al., 2003; Chabalala et al., 2020). However, they often fall short in elucidating the fundamental geological controls—especially the intricate interplay between primary lithofabric developed during deposition and subsequent structural modification (folding, faulting, uplift)—that govern the ultimate preservation capacity and determine the final gas content distribution within highly deformed, heterogeneous shale sequences (Guo et al., 2017; Algeo and Lyons, 2006). Understanding these interactions within specific structural settings (e.g., box folds vs arcuate anticlines vs remnant synclines) is crucial for predicting preservation likelihood and developing effective exploration strategies in structurally complex terrains (He et al., 2025).

This paper aims to address this gap by investigating the multi-sphere coupling characteristics and gas-bearing controlling factors of the Lower Carboniferous Dawuba Formation shales specifically within the tectonically complex YZLA. Our research focuses on deciphering how the interplay between the unique depositional heterogeneity (particularly the "thin interbedded" mudstone-limestone fabric) and the region's intricate tectonic history influences shale gas preservation. By integrating analyses of mineral composition, organic geochemistry, reservoir characteristics (porosity, permeability, micro-fractures), and measured gas content data, we seek to identify the dominant factors controlling gas retention in this challenging geological setting. This study contributes to the broader international understanding of shale gas preservation mechanisms in complex tectonic zones by providing a detailed case study of how deposit.

2 Geological background

The marine strata of the Lower Carboniferous in southern China have undergone multiple tectonic events since their initial deposition in the early Carboniferous (Gallego-Torres et al., 2010; Srinivasan et al., 2021; Scott et al., 2005), a process deeply intertwined with the coupling of tectonic-climatic-oceanic multiple spheres. A prime example is the YZLA, a northwest-oriented aulacogen situated in the southwestern part of Guizhou Province. This fault belt is an important tectonic feature in the southern region of the Upper Yangtze Plate (Figure 1a), with a length of about 400 km and a width ranging from 10 to 80 km (Wang et al., 2018), not only shaped the regional tectonic framework but also influenced climatic patterns and oceanic circulation. It serves as a significant boundary fault between various tectonic units, such as the northern Yunnan-Guizhou depression, the central Guizhou uplift, the southern Guizhou depression, the southwestern Guizhou depression, the eastern Guizhou uplift, and the Nanpanjiang depression. From the Devonian to the end of the Permian, the study area experienced five stages of tectonic evolution (Loucks et al., 2012; Yuan et al., 2017): extension-rifting, faulting, rift valley development, weakening-tectonic inversion, and intracontinental contraction. Each stage reflected dynamic interactions among tectonic uplift/subsidence, climatic shifts (e.g., monsoon intensity, evaporation-precipitation balance), and oceanic responses (e.g., sea-level fluctuations, anoxic basin formation). For instance, the basin-controlling faults of the late Paleozoic extensional rifts not only bounded a fan-shaped backthrust structure in the shallow crust but also modulated oceanic water mass exchange, influencing the deposition of organic-rich shales. As a result, the Carboniferous strata, shaped by this multi-sphere coupling, are now shallowly buried and in close proximity to the erosion zone (Milliken et al., 2013; Jones and Manning, 1994), highlighting the lasting impact of tectonic-climatic-oceanic interactions on regional stratigraphy and reservoir preservation.

The study area can be divided into three sections from north to south based on the structural changes along the strike of the YZLA (Chen et al., 1994; Xia et al., 1995; Cheng and Xu, 1998; Liu et al., 2016). The northwest section, stretching from the Weining area to the Liupanshui area, is characterized by four deep faults and a transition from a carbonate platform to a carbonate slope (Cheng and Xu, 1998). The middle section, from the Liuzhi area to the Guanling area, features two deep faults and is mainly composed of deep-water shelf deposits. The southeast section, from the Ziyun area to the Luodian area, evolves into one deep fault, with a change in the main dip direction of the normal faults from west-south to northeast, and a transition from mudstone slope to shale deep-water deposits (Yuan et al., 2019; Ji et al., 2012). The Dawuba Formation in this area is predominantly made up of platform, slope, and deep-water basin deposits (Figure 1b), resulting in a complex sedimentary pattern with diverse lithology combinations across different regions.

3 Experimental method

3.1 Sample selection

This study is intended to reveal the shale development characteristics of the Lower Carboniferous Dawuba Formation in the YZLA and to explore the main controlling factors and gas content of the shale. Thorough tests and analyses were performed on core samples from wells QSD1 and QZY1, covering aspects such as petrology, organic geochemistry, reservoir properties, and gas content. Moreover, samples from more than 10 typical sections, including the Manchang section, Getu River section, and Shuicheng section, were supplemented to show the shale characteristics of different areas. The lithologies of the samples in this study mainly consist of mudstone, shale, limestone, and argillaceous limestone, spanning various parts of the Dawuba Formation from bottom to top. A total of 150 outcrop samples and more than 200 core samples were collected. The experimental work was mainly carried out by the National Geological Experimental Testing Center and Sichuan Keyuan Engineering Technology Testing Center Co., Ltd.

3.2 Mineral composition analysis

The mineral composition and content of the shale samples from the Dawuba Formation were identified through XRD (X-ray diffraction) analysis. The samples were crushed to a size smaller than 300 mesh, mixed with ethanol, and coated onto glass slides to ensure uniformity of the sample surface. Thereafter, the samples were scanned using a Panalytical X'Pert Powder diffractometer (supplied by the Netherlands), fitted with a copper X-ray tube, at 40 kV and 30 mA, within the range of 2°–70°. By fine-tuning the scanner parameters and sample positions, diffraction data reflecting the crystal structure and arrangement were generated. The diffraction data were processed and analyzed with Jade software, resulting in semi-quantitative outcomes of the relative mineral content. This enabled the determination of the relative percentages of the major minerals and provided an understanding of the overall mineral composition characteristics. In the final step, the polished samples were analyzed using emission white light and fluorescence microscopy at 24°C to confirm and assist in determining the mineral composition.

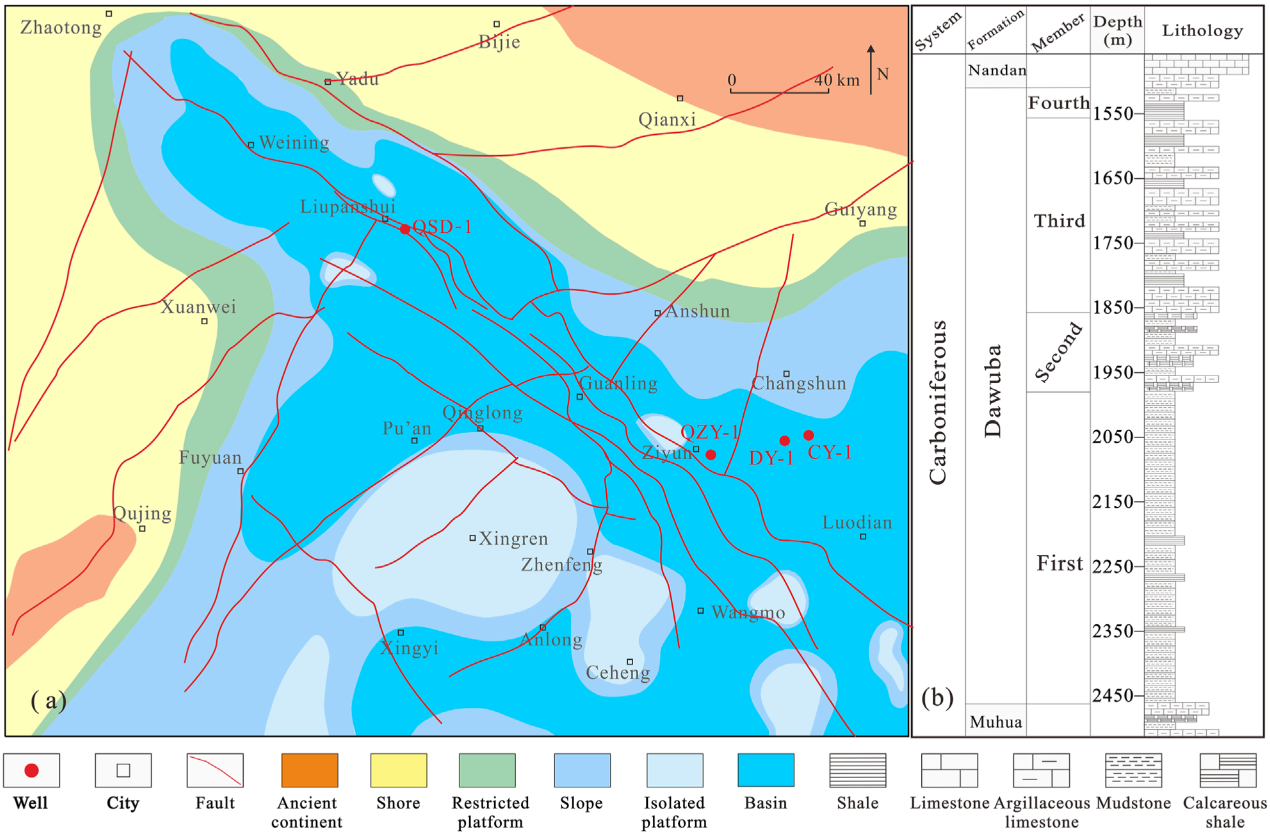

FIGURE 1
Regional tectonic setting and sedimentary facies of the study area during the Early Carboniferous **(a)**, Lithological characteristics of the Early Carboniferous Dawuba Formation in well QSD1 **(b)**.

3.3 Organic carbon content

The organic carbon content of the samples was measured using a Leco-CS-744 carbon-sulfur analyzer (from the United States). The procedure involved initial sample pre-treatment, where the samples were weighed and their weights recorded. Subsequently, inorganic carbon was removed using a dilute hydrochloric acid solution, followed by thorough washing and drying. The dried samples were then mixed with combustion aids (iron and tungsten combustion aids) to convert organic carbon compounds into carbon dioxide. Finally, a thermal conductivity detector was employed to detect and determine the total organic carbon content.

3.4 Organic matter type

The types of organic matter were examined using an optical microscope. Specifically, a Zeiss Axio Scope. A1 polarizing microscope (from Germany) equipped with a TIDAS S-800 spectrophotometer (from Germany) was utilized to measure the random reflectance of vitrinite at a wavelength of 546 nm. To ensure result accuracy, equipment calibration was performed, and the accuracy was verified using two standard samples with known reflectance values. Over 20 measurement points were taken in the samples to guarantee the reliability and representativeness of the measurements.

3.5 Thermal maturity

Vitrinite reflectance was employed to assess the thermal maturity of the formations. A Zeiss Axio Scope. A1 polarizing microscope (from Germany) and a TIDAS S-800 microspectrophotometer (from Germany) were used to measure the Ro values in both reflection and fluorescence modes. Initial equipment calibration was conducted, and accuracy was confirmed using standard samples with known reflectance. The samples were polished, and oil immersion was applied. Multiple Ro value measurements were taken in appropriate areas and averaged to provide precise information about the thermal maturity of the formations.

3.6 SEM observation

The minerals and micropores in the Dawuba Formation shale were investigated using a ZEISS Sigma300 scanning electron microscope (from Germany) and a Bruker Quantax 200G energy dispersive spectrometer (from Germany). The samples were prepared by treating them with a GATAN Model 685. C argon ion polisher (from the United States) to achieve a smooth surface. They were then coated with a gold film approximately 10 nm thick to enhance conductivity and imaging resolution. Observations were carried out at a temperature of 24°C and a humidity of 35%, with an operating voltage of 15 kV. The electron microscope was used to examine the microscopic structures, pore distribution, and crack distribution of the shale. Energy spectrum data were collected for the analysis of mineral composition and micropore structures.

3.7 3D-FIB SEM observation

A Zeiss Crossbeam 540 FIB-SEM (from Germany) was utilized for the observation and three-dimensional sectioning of shale samples. The sample preparation process included selecting representative areas, mechanical grinding, and argon ion polishing. During SEM observation, the backscattered electron mode was employed, and specific areas underwent three-dimensional sectioning to observe the developmental characteristics of organic matter. The ion beam cutting process involved a working voltage of 30 kV, an ion beam current of 700 pA, and an acceleration voltage of 2 kV for the electron beam, with a current of 180 pA. Avizo software was used for the segmentation and three-dimensional reconstruction of FIB-SEM images to analyze the microstructure of shale. In data processing, image segmentation was performed using a threshold tool, and the Avizo Pore Network Model (PNM) module was applied to calculate the parameters of pores and throats.

3.8 Gas desorption

The gas content of shale was measured in the field using an automated desorption instrument YYHQ-III (from China) and the drainage desorption method. The desorption procedure consisted of the following steps: collecting 2.0–4.0 kg whole-diameter rock samples, removing mud, weighing the samples, and placing them into a metal desorption vessel filled with 200-mesh quartz sand. The vessel was sealed tightly. During the desorption process, desorption was carried out under the temperature condition of mud circulation for 3 h, followed by high-temperature rapid desorption at the formation temperature until complete desorption was achieved. The drainage desorption method was used under atmospheric pressure, with gas samples collected every 30 min, requiring a minimum gas volume of 50 mL. After collecting the gas samples, the liquid level was adjusted, and the gas inside the sealed measuring cylinder was drained to prepare for subsequent desorption and gas collection. The collected desorbed gas samples were sealed upside down in bottles during storage and transportation, with the bottom water preserved. The volume of the desorbed gas was measured and converted to standard conditions (20°C, 101.325 kPa). The loss of gas during the desorption process was regressed using the United States Bureau of Mines (USBM) linear method to obtain accurate results.

3.9 Poisson's ratio

During drilling, the eclips-5700 logging system was used to carry out orthogonal multipole array acoustic logging. The XMAC-II array waveform was processed by the slowness time coherence (STC) technology, from which the P-wave, S-wave and Stoneley wave waveforms of the formation were extracted, and the slowness of each waveform was calculated. Based on waveaven program of Xpress interpretation system, the time difference of longitudinal wave (DTC), time difference of transverse wave (DTS) and time difference of Stoneley wave (dtst) are further extracted from the unipolar source waveform, and the corresponding TTC, TTS and ttst are obtained at the same time. Finally, through the mechprop program of Xpress interpretation system, the extracted P/S wave moveout, conventional density curve, porosity and lithologic content calculated based on density data and other parameters are input, and the petrophysical parameters such as P/S wave velocity ratio, Poisson's ratio, bulk modulus, shear modulus and Young's modulus are calculated, providing data support for the analysis of reservoir mechanical properties.

3.10 Minimum/maximum horizontal principal stresses

Based on the orthogonal multipole array acoustic logging data, the calculation of horizontal principal stress needs to integrate the rock mechanics parameters and the theoretical framework of *in-situ* stress. Firstly, the rock elastic parameters such as Poisson's ratio and Young's modulus are calculated by using the P-wave, S-wave moveout and density logging data obtained from acoustic logging; Secondly, the overburden pressure is calculated by integrating the density logging data, and the vertical effective stress is derived based on the measured results of pore pressure; Then, based on the assumption of plane strain state, combined with the elastic theory, a model is built through the vertical effective stress and elastic parameters to estimate the horizontal principal stress, in which the structural additional stress component is corrected by relying on the regional geological background or the characteristics of borehole collapse and induced fractures identified by imaging logging; Finally, the imaging logging is used to analyze the long axis of borehole wall collapse or the direction of induced fracture, determine the direction of the maximum and minimum horizontal principal stress, and calibrate the calculation results through the fracturing test data, so as to obtain reliable horizontal principal stress parameters, which provides a key basis for reservoir engineering analysis.

3.11 Total hydrocarbon content

SL-ALS-2.2 comprehensive logging instrument is used for gas logging in drilling operation, with the gas chromatograph serving as the core component for separating and analyzing multi-component mixed gases. During the process, gas chromatographic analysis of drilling fluid samples is conducted every 1 m to measure methane through pentane fractions, and total hydrocarbon content is normalized to formation depth and lithology. The working principle is as follows: after sample gas is injected into the chromatographic column, components in the mixed gas migrate at different rates under carrier gas due to differences in their distribution coefficients on the column's stationary phase, achieving efficient separation. The separated components then enter the detector sequentially; by recording each component's peak time (retention time) and peak area, the gas composition and content can be accurately analyzed.

4 Geologic characteristics of carboniferous shales

4.1 Northwestern region of YZLA

Liupanshui area is located in the northwest section of YZLA, and Well QSD1 is a typical well in this region. The first member at the base of the Dawuba Formation in this well is predominantly composed of dark gray mudstone and argillaceous limestone, with local interbedding of mudstone and limestone. The second member is mainly composed of dark gray argillaceous limestone and mudstone interbedded with shale. The third member is primarily composed of argillaceous limestone interbedded with mudstone and shale. The fourth member is mainly composed of argillaceous limestone, limestone, and bioclastic limestone (Figure 2). The clay content gradually decreases, while the calcite content and the content of brittle minerals gradually increase from the first to the fourth member (Nie et al., 2009; Wang, 2016). The types of organic matter are mainly Type III and Type II_2, with an average total organic carbon (TOC) of 0.79%, ranging from 0.09% to 1.70%. The field desorption gas content of the first member can reach up to 5 m^3/t, but it has poor preservation conditions, as indicated by more than 60% of air in the original gas composition (with a nitrogen to oxygen ratio of approximately 4:1), and a poor lithology superposition relationship (the thickness difference between shale and argillaceous limestone is large, and the single layer thickness is either too thick (more than 5 m) or too thin (less than 0.5 m)). The upper part of the first member and the second member (1,600 m–1,950 m) have good preservation conditions, as indicated by relatively more enriched organic matter, with an average vitrinite reflectance (R_o) of 2.19%, frequent interbedding of shale and argillaceous limestone, a mudstone-to-argillaceous limestone ratio close to 1:1, single layer thickness less than 5 m, which is a good lithology superposition section (the thickness of shale and argillaceous limestone is similar, and the single layer thickness ranges from 0.5 m to 5 m), and an average field desorption gas content of 1.6 m^3/t (Yuan et al., 2017), with methane content exceeding 60% in the gas composition. The total hydrocarbon content ranges from 0% to 63.41%, with an average of 9.15%, as shown by the gas logging.

4.2 Middle region of YZLA

The middle section of the YZLA runs from Liuzhi County to Guanling County in Guizhou Province, connecting with the southern Guizhou depression to the northeast and the southwestern Guizhou depression to the southwest. The Dawuba Formation within this stretch is notable for its considerable burial depth, going beyond 6,000 m in the rift valley and 3,500 m on the slope. For example, well AS1 located in the slope area has a burial depth of about 4,700 m and a thin thickness of less than 100 m, without the development of bottom shale (Peng et al., 2000; Yuan et al., 2018). In accordance with the interpretation results of the wide-area electromagnetic method, a deep-water sedimentary center influenced by NW-oriented faults is present in the Guanling area of the rift valley, where there is presently no drilling data. The shale thickness of the Dawuba Formation in this region is roughly 450 m. This area is distinguished by a low degree of fault development and relatively simple tectonic conditions.

4.3 Southeastern region of YZLA

4.3.1 Deep-water sedimentary area

The southeastern section of the YZLA comprises a deep-water sedimentary area and a slope sedimentary area near the Ziyun region. The deep-water sedimentary area is typified by well QZY1, where the Dawuba Formation mainly consists of argillaceous limestone and shale, with interbeds of gray-black thin-layered siliceous rocks (Figure 2). The Dawuba Formation can be divided into four members from the base. The first member exhibits significant lithological changes, with mudstone and shale in the upper part, limestone interbedded with thin-layer shale in the middle part, and argillaceous limestone and mudstone with uneven thickness interbeds in the lower part. This section is characterized by a high field desorption gas content, and fractures along with fracture zones are extremely well-developed. The second member is mainly composed of argillaceous limestone and mudstone with uneven thickness interbeds. The third member primarily consists of gray-black mudstone and shale, alternating with argillaceous limestone, with high mud content and numerous high-angle shear fractures visible. The fourth member shows alternating development of argillaceous limestone and mudstone. The first and fourth members have a higher proportion of limestone, while the middle second and third members generally have increased mud content. Strawberry-shaped pyrite, with a particle size of 10–20 μm, is commonly found in the mudstone section, indicating a deep-water reducing sedimentary environment. The calcite content gradually increases from the first to the fourth member, while the clay mineral and quartz content gradually decreases. The clay minerals have a high illite/montmorillonite mixed layer content. The porosity is about 3%, and the permeability is approximately 0.4 mD. The organic matter types are all type II_2, with an average TOC of 1.45%, ranging from 0.54% to 2.64%. The first and third members of the Dawuba Formation have relatively more enriched organic matter, with TOC greater than 2%. Ro averages 3.5%, and the field desorption gas content averages 1.0 m^3/t (Peng et al., 2000; Yuan et al., 2017; 2018; 2022). The gas composition of the third member is mainly nitrogen, with a high nitrogen content of 70% and an oxygen content of 10%. However, the methane content of the first member (2,900 m–2980 m) exceeds 75%, and it has a good lithology superposition relationship. The total hydrocarbon content ranges from 0.01% to 1.97%, with an average of 0.23%, as indicated by the gas logging (Yang et al., 2019; Liu et al., 2006).

4.3.2 Slope sedimentary area

The slope area is mainly distributed in the regions near Huisui-Changshun and Luodian area, with well CY1 and DY1

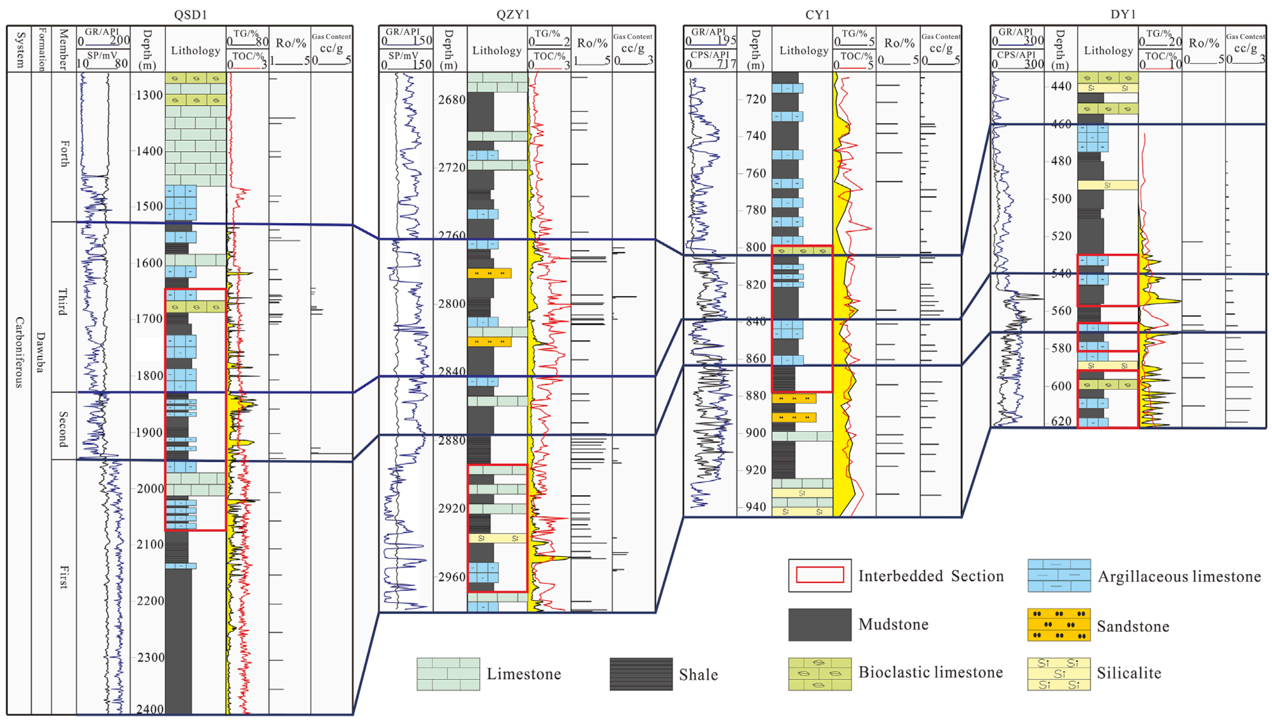

FIGURE 2
Cross-well profiles of lithology, TOC and gas content in different parts of YZLA.

as representative wells (Figure 2). In well CY1, the Dawuba Formation consists of four members from bottom to top: the first member mainly comprises shale, with interbeds of pyrite nodules and gray-black argillaceous limestone nodules; the second member is primarily composed of argillaceous limestone and calcareous mudstone, exhibiting horizontal bedding; the third member mainly consists of mudstone and argillaceous limestone, with a small amount of argillaceous limestone strips; the fourth member is mainly made up of calcareous mudstone and thin-layered argillaceous limestone, containing abundant brachiopod, crinoid stem fossil fragments, and stellate pyrite particles. The silicate mineral content decreases initially and then remains relatively stable from bottom to top, while the carbonate mineral content decreases first, then increases, and subsequently decreases from bottom to top. The clay mineral content increases initially and then decreases, with sections having high clay mineral content exhibiting high field desorption gas content. The second and third members have better lithology superposition sections, with a gas content of about 2.5 m^3/t (Yang et al., 2021; Li et al., 2022b). The porosity is approximately 2.4%, and the permeability is about 0.005 mD. The organic matter is mainly type II_2 and type III, with an average TOC of 1.79%, ranging from 0.21% to 4.51%. The third member has relatively more enriched organic matter. Ro ranges from 2.13% to 3.27%, with an average of 2.66%, and is generally over-mature.

Well DY1 also divides the Dawuba Formation into four members. The first member mainly consists of argillaceous limestone, with interbeds of a small amount of thin-layered bioclastic limestone and siliceous rocks; the second member is primarily composed of calcareous mudstone and shale; the third member mainly comprises calcareous mudstone, shale, and argillaceous limestone, with thin-layer siliceous shale interbeds; the fourth member is mainly made up of mudstone and bioclastic limestone, with thin-layered siliceous rocks. Coral, brachiopod, and crinoid stem fossils are common, along with a small amount of pyrite strips and horizontal striations. Organic matter types I to III are all developed, with a predominance of type II_2. TOC ranges from 0.41% to 6.93%, with an average of 2.19%. The first and second members (530m–620 m) have more enriched organic matter. Ro ranges from 2.15% to 2.66%, with an average of 2.43%, and is over-mature. In the first and second members, sections with frequent interbedding of mudstone and limestone and high clay mineral content have high field desorption gas content, belonging to better lithology superposition sections, reaching up to 2.5 m^3/t (Figure 2), with methane content above 60%. The gas logging indicates that the total hydrocarbon content ranges from 0.33% to 19.92%, with an average of 4.17%.

5 Discussion

5.1 Comparison of interbedded and thick-bedded section

The Early Carboniferous Dawuba Formation is made up of gray-black shale, gray-black dense limestone, argillaceous limestone, silty shale interbedded with thin-layer flint, and minor silty sandstone and siliceous shale strata, distributed across different regions of the YZLA. Based on lithology combinations, the Dawuba Formation

TABLE 1 Characteristics table of the interbedded section and the thick-bedded section.

Lithology combinations type	Interbedded section		Thick-bedded section	
Evaluation level	Excellent	Good	Medium	Poor
Lithological combination characteristics	Mudstone-to-argillaceous limestone Ratio 1:1 ~ 1:1.5 Combined thickness 0.5 ~ 5 m	Mudstone-to-argillaceous limestone Ratio 1:1.5 ~ 1:2 Combined thickness 5 ~ 10 m	Mudstone-to-argillaceous limestone Ratio 1:2 ~ 1:5 Combined thickness 5 ~ 10 m	Mudstone-to-argillaceous limestone Ratio >1:5 Combined thickness >10 m or <0.5 m
Lithological combination and gas bearing characteristics	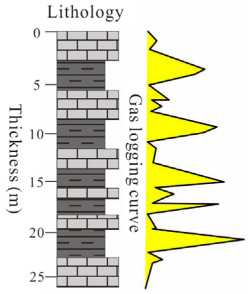	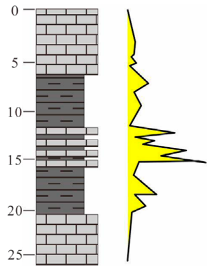	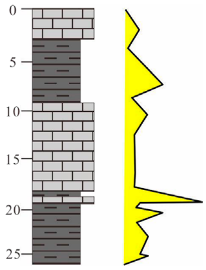	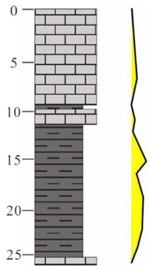

, Argillaceous limestone
, Mudstone.

can be divided into four members (Zheng et al., 2022; Wang et al., 2024; Bai et al., 2018). However, from a broader perspective, it can be categorized into two types of lithology combinations (Table 1). The "interbedded section" is characterized by the frequent interlayering of mudstone and argillaceous limestone. Within this section, the mudstone-to-argillaceous limestone ratio varies from 1:1 to 1:2, and the cumulative thickness of these interlayered beds spans from 0.5 m to 10 m. Conversely, the "thick-bedded section" is composed of thick strata of either mudstone or limestone. In this case, the ratio of mudstone to argillaceous limestone exceeds 1:2. Moreover, the combined thickness of the layers is either notably thick (greater than 10 m) or remarkably thin (less than 0.5 m). These two lithology combinations have distinct impacts on reservoir physical properties, gas-bearing characteristics, and other features, as well as different implications for sedimentary environments and accumulation conditions.

The interbedded section is characterized by frequent interbedding of mudstone and argillaceous limestone (Figure 3a), with a single layer thickness ranging from 0.5 m to 5 m and a small thickness difference between mud shale and argillaceous limestone. The mudstone-to-argillaceous limestone ratio is between 1:1 and 1:2 (Figures 3c,d). This lithology combination indicates rapid changes and high-energy events in the deep-water sedimentary environment. The interbedded section has better reservoir physical properties, with a higher field desorption gas content of about 2.5 m^3/t. The porosity is approximately 2.9%, and the permeability is around 0.005 mD. The organic matter is mainly type II_2 and type III, with an average TOC of 1.79%, ranging from 0.21% to 4.51%, and an average Ro of 2.66%, ranging from 2.13% to 3.27%.

The thick-bedded section consists of mudstone and argillaceous limestone interbedding (Figure 3b), with a single layer thickness that is either too thick (greater than 5 m) or too thin (less than 0.5 m), and a large thickness difference between mud shale and argillaceous limestone (Figures 3e,f). The mudstone-to-argillaceous limestone ratio is between 1:2 and 1:5. This lithology combination indicates stable sedimentation or low-energy events in the deep-water sedimentary environment. The thick-bedded section has worse reservoir physical properties, with a lower field desorption gas content. The porosity is relatively low at about 2.0%, and the permeability is approximately 0.005 mD.

According to the above classification, in well QZY1, the first member of the Dawuba Formation is the main part of the "interbedded section," with frequent interbedding of mudstone and argillaceous limestone. The ratio of mudstone to argillaceous limestone is about 1:1.1, indicating rapid changes associated with high-energy processes such as turbidite flows, storm-induced resedimentation, or density current activities in the deep-water sedimentary environment. The second, third, and fourth members are the main parts of the "thick-bedded section," with unequal thickness interbedding of argillaceous limestone and mudstone. The ratio of mudstone to argillaceous limestone is greater than 1:5, indicating stable sedimentation or low-energy events in the deep-water sedimentary environment. In well QSD1, the first member is primarily composed of black mudstone in the "thick-bedded section," accounting for more than 90% of the strata, indicating stable sedimentation or low-energy events in the deep-water sedimentary environment. The second and third members are the main parts of the "interbedded section" in this well, with frequent interbedding of mudstone and argillaceous limestone. The ratio of mudstone to argillaceous limestone is about 1:1.1 to 1:1.5, indicating rapid depositional shifts linked to high-energy processes such as turbidite flows, storm-induced resedimentation, or density current activities in the deep-water sedimentary environment. By contrast, the fourth member exhibits a higher argillaceous limestone content, with a mudstone-to-argillaceous limestone ratio of approximately 1:2.1, reflecting stable sedimentation dominated

FIGURE 3
Lithofacies associations of well QZY1 in the interbedded section (gray lines represent mudstone and shale, blue lines represent argillaceous limestone and limestone) **(a)**; Lithofacies associations of well QZY1 in the thick-bedded section **(b)**; Thin interbedding features of mudstone and argillaceous limestone **(c,d)**; Mudstone bands developed in thick limestone **(e)**, Thick blocky mudstone **(f)**, Irregular calcite bands developed in calcareous mudstone **(g)**, Interbedding of mudstone and argillaceous limestone, and microcrystalline limestone is common **(h)**, Clay minerals dispersed in micrite **(i)**, Clay mineral aggregates developed in micrite **(j)**.

by low-energy processes like suspension settling or background hemipelagic deposition in the same deep-water setting.

5.2 Reservoir features of interbedded section

The "interbedded section" of the Dawuba Formation is marked by the frequent interbedding of mudstone and argillaceous limestone, which signifies rapid changes and high-energy events in the deep-water sedimentary environment. The interbedded section displays evident interbedding features that can be observed in both core samples and thin sections, and these features can be classified as follows.

(1) A structure characterized by the interbedding of mud crystal calcite and clay minerals, formed by the incorporation of microcrystalline clay mineral aggregates into mud crystal calcite (Figure 3g). The clay minerals mainly comprise illite, kaolinite, and montmorillonite, which considerably affect the reservoir's physical properties and gas-bearing characteristics (Jiang et al., 2010; Ma et al., 2022b).

(2) A thin-layered or striped structure resulting from the interbedding of microcrystalline sandstone limestone and carbonaceous mudstone (Figure 3h). The microcrystalline sandstone limestone has a granular structure, with fine sand grains as the predominant particle type, followed by bioclasts such as coral, brachiopod, and crinoid stem. The fine sand grains are fragmental, rounded, or irregular in shape and are composed of microcrystalline carbonate. The carbonaceous mudstone is formed of clay minerals and carbonaceous matter, with a cryptocrystalline structure and a black or gray-black color.

(3) A high-angle fracture or veinlet structure created by the interbedding of argillaceous limestone and calcite veins. The argillaceous limestone consists of microcrystalline calcite and a small amount of clay minerals, exhibiting a mud crystal or mud granular structure. The calcite vein is made up of large-crystal calcite, with a smooth fracture or surface and a white or light gray color.

The pore structures of the interbedded section and the thick-bedded section differ notably, as shown by scanning electron microscopy (Figure 4). The key differences are as follows.

(1) The interbedded section has more developed clay mineral seams (Figures 4a,c), which generate secondary pore spaces (Zeng et al., 1992). These seams are the tiny gaps between clay mineral particles or other particles,

typically nanometer-sized, and contribute to the reservoir's permeability.

(2) The interbedded section better preserves dissolution pores, thereby enhancing the reservoir's effective porosity (Figure 4b). Dissolution pores are secondary pores formed by the dissolution of carbonate or siliceous rocks by formation fluids or groundwater. They are usually micrometer-sized and significantly influence the reservoir's gas-bearing capacity.

(3) The interbedded section has superior pore connectivity, which aids in the migration and accumulation of gas. Pore connectivity refers to the degree of interconnection between pores of different types and scales within the reservoir. It determines the reservoir's permeability and gas-bearing capacity.

(4) The interbedded section predominantly features open micro-fractures (Figures 4d–f), which remain unclosed due to compaction. These micro-fractures are secondary fractures formed by formation stress or tectonic activity. They are typically millimeter-sized and notably improve the reservoir's permeability and gas content.

5.3 Gas content features of interbedded section

The gas content of shale is a key parameter for evaluating shale gas resource potential. The well correlation diagram indicates that the interbedded section of shale has a higher gas content than the thick-bedded section. Given that direct gas-bearing property test data from drilling are insufficient to cover the entire well interval, total hydrocarbon content from gas logging are used as an indirect indicator of subsurface gas-bearing conditions, allowing for a preliminary assessment of gas content in different lithological combinations. To further investigate their relationship, we compared the gas logging curve with TOC, porosity, clay mineral content, and rock mechanics-related parameters (Poisson's ratio, maximum horizontal principal stress, minimum horizontal principal stress) (Figure 5), and analyzed their correlations with total hydrocarbon content. The data analysis leads to the following conclusions:

The gas content of shale is a key parameter for evaluating shale gas resource potential. The well correlation diagram indicates that the interbedded section of shale has a higher gas content than the thick-bedded section. To further investigate their relationship, we compared the gas logging curve with TOC, porosity, clay mineral content, and rock mechanics-related parameters (Poisson's ratio, maximum horizontal principal stress, minimum horizontal principal stress) (Figure 5). We also analyzed their relationship with the total hydrocarbon content. The data analysis results in the following conclusions.

(1) The lithologic interbedded section has a much higher shale gas content than the thick-bedded section, implying that it has more favorable shale gas preservation conditions. Gas content is positively related to clay mineral content in the lithologic interbedded section, possibly because clay mineral fissures create some secondary pore space, enhancing the reservoir permeability and gas content. Gas content is also positively associated with mechanical parameters such as Poisson's ratio, maximum/minimum horizontal stress, *etc.*, in the lithologic interbedded section, possibly because high-angle fractures or veins are formed in the limestone interlayers under stress transformation, increasing the pore connectivity and free gas storage space.

(2) The gas content of shale is not directly determined by the TOC, indicating that organic matter adsorption has a minor effect on shale gas content, whereas gas mainly occurs as free gas in the mineral pores and fractures (Dong et al., 2017). The interbedded section does not show a clear relationship between gas content and TOC (Figure 5e), but it has a higher gas content than the thick-bedded section. This suggests that shale gas content is primarily determined by the preservation conditions of the interbedded section, rather than by organic matter adsorption.

(3) Gas content and porosity exhibit a low correlation (Figure 5f), possibly because intense tectonic activity disrupted the initial preservation conditions of shale gas, leading to significant alterations and redistribution of the original gas content. Therefore, porosity has a minor impact on shale gas content in complex tectonic areas. Porosity partly indicates the effective porosity of the reservoir, but it does not fully correspond to it, as the reservoir also contains secondary pores and fractures of various types and sizes.

(4) Quartz, clay minerals, and gas content are not clearly correlated, which may result from the complex tectonic movement damage that the shale gas reservoir experienced. This reduced the influence of mineral composition on shale gas content. However, overall, under similar mineral composition conditions, the interbedded section has a higher total hydrocarbon content than the thick-bedded section (Figure 5A).

5.4 Preservation condition

The YZLA significantly impacted the tectonic transformation of the southern part of the Yangtze Plate in two distinct tectonic stages: the late Paleozoic and the late Indosinian. During the late Paleozoic, it acted as the boundary between the cratonic margin rift basin and the cratonic intra-basin on the southern edge of the Yangtze Plate, indicating a tectonic extension environment at that time. Since the late Indosinian, however, it has become the mechanical boundary between the cratonic margin compressional basin and the cratonic intra-basin, indicating a tectonic compression environment at that time.

Tectonic uplift and erosion greatly affected the preservation of strata. As the target layer approached closer to the erosion zone, the shale gas preservation conditions deteriorated. The macroscopic tectonic background was also evident at the microscopic level. Under the microscope, numerous rock veins were observed in the Dawuba Formation shale strata in the study area, interwoven into a network structure with multi-stage cutting features. Some organic matter also filled the rock fractures (Figure 6).

Based on the typical wells in the study area, this study found that TOC had no direct influence on the high gas content shown by gas logging wells. Instead, gas content was strongly correlated with the

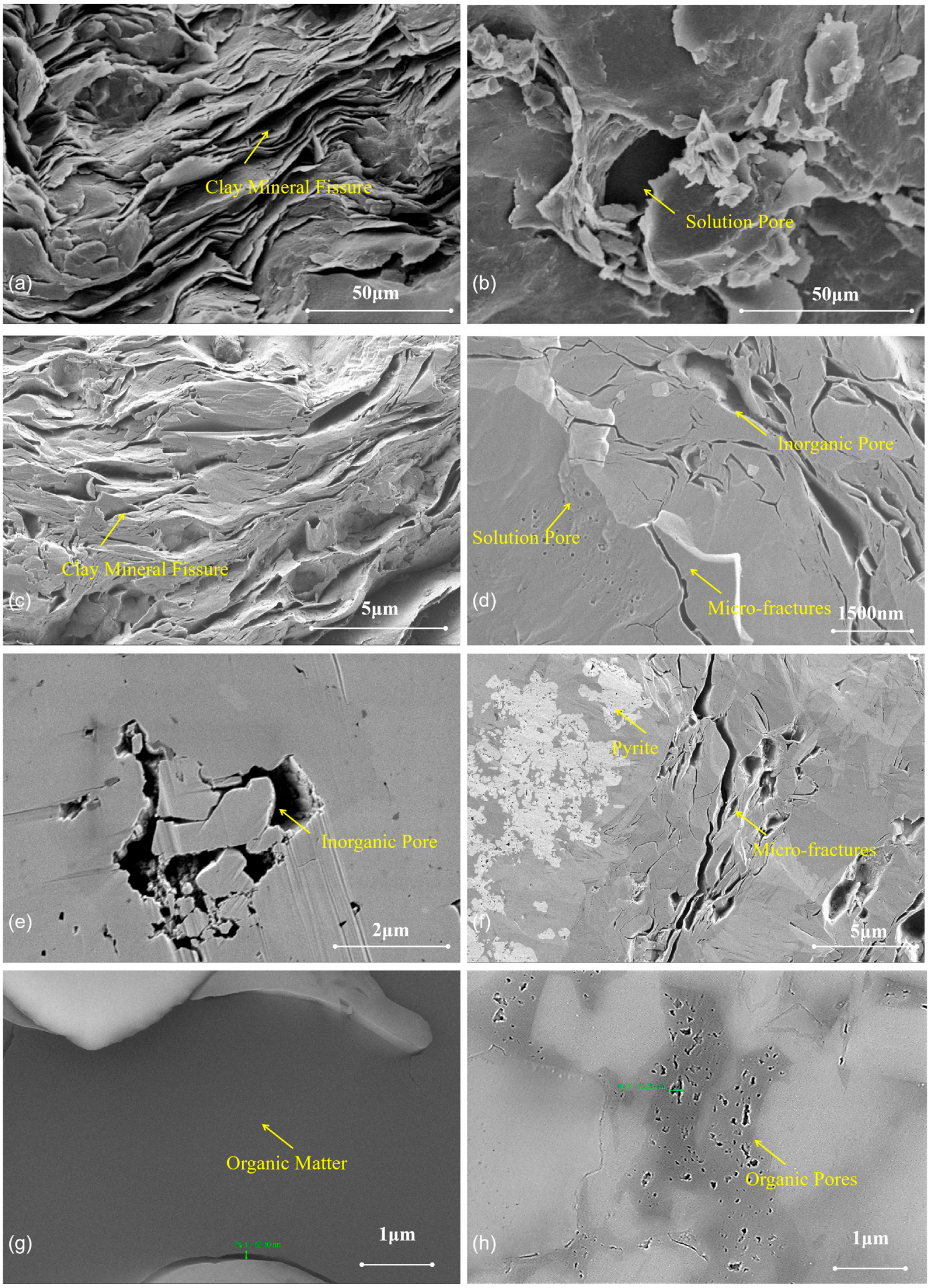

FIGURE 4
Microstructure of shale samples from Dawuba Formation in YZLA. **(a)** Black shale in the interbedded section of Shuangshui area, clay mineral fissures developed. **(b)** Black argillaceous limestone in the interbedded section of Lanba area, solution pores. **(c)** Black shale in the interbedded section of well QSD1, clay mineral fissures developed. **(d)** Black shale in the interbedded section of well QSD1, clay mineral fissures and micro-fractures developed, abundant solution pores. **(e)** Black mudstone in the interbedded section of well QSD1, large amount of inoranic pores, good connectivity. **(f)** Black shale in the interbedded section of well QSD1, pyrite and micro-fractures developed. **(g)** Black shale in the thick-bedded section of well QZY1, organic pores rarely development. **(h)** Black shale in the interbedded section of well QZY1, organic pore developed.

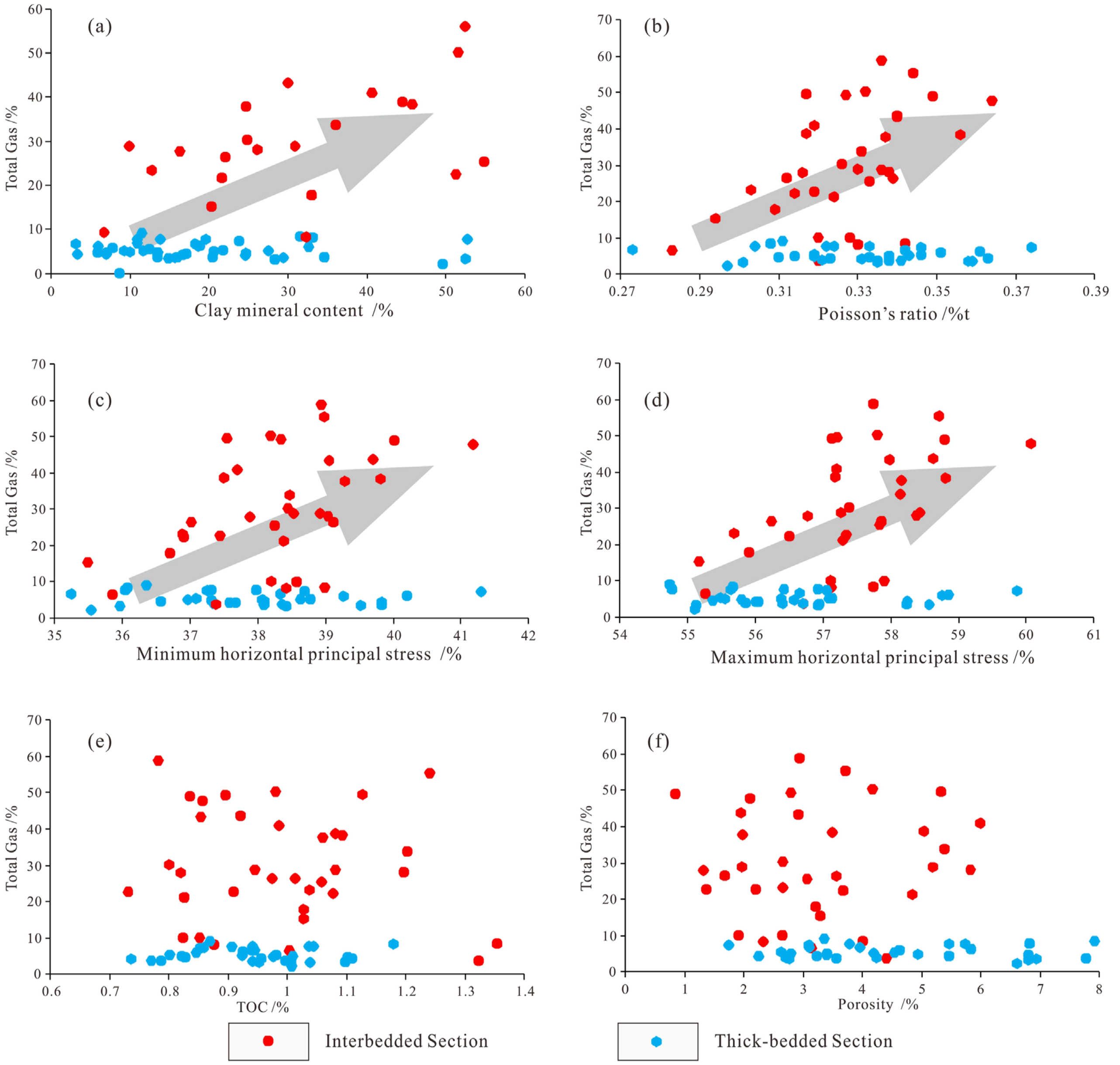

FIGURE 5
Comparative analysis of gas content with **(a)** clay content, **(b)** Poisson's ratio, **(c)** minimum horizontal principal stress, **(d)** maximum horizontal principal stress, **(e)** TOC, and **(f)** porosity in the interbedded and thick-bedded sections of Well QSD1.

mudstone-to-argillaceous limestone ratio, micro-fractures, and the development degree of clay interlayer fissures (Figure 7). The shale gas content reached its peak when the lithologic interbedded section coincided with the position of micro-fracture development.

It was found that the shale strata of the Dawuba Formation mainly contain free gas, and the preservation conditions play a critical role in gas retention. Specifically, the mudstone in the interbedded section effectively supports the micro-fractures in the shale strata. This support widens the fractures and increases the pore volume, thereby providing ample storage space for free gas. As a result, the interbedded section has a significantly higher gas content compared to the thick-bedded section.

The thick-bedded section refers to the lithology combination of mudstone and argillaceous limestone interbedding, with a single layer thickness that is either too thick (greater than 5 m) or too thin (less than 0.5 m). After hydrocarbon generation, the thick-bedded section experienced increased pressure, causing oil and gas to migrate to the mudstone in the gray-mud interbedded section. The mud shale in the "thick-bedded section" had strong plasticity and weak compressive strength, so micro-fractures tended to close after hydrocarbon expulsion, reducing pores and storage space. In contrast, for the gray mudstone "interbedded section", due to its high calcium content, it was more prone to form micro-fractures, which could be effectively blocked by denser

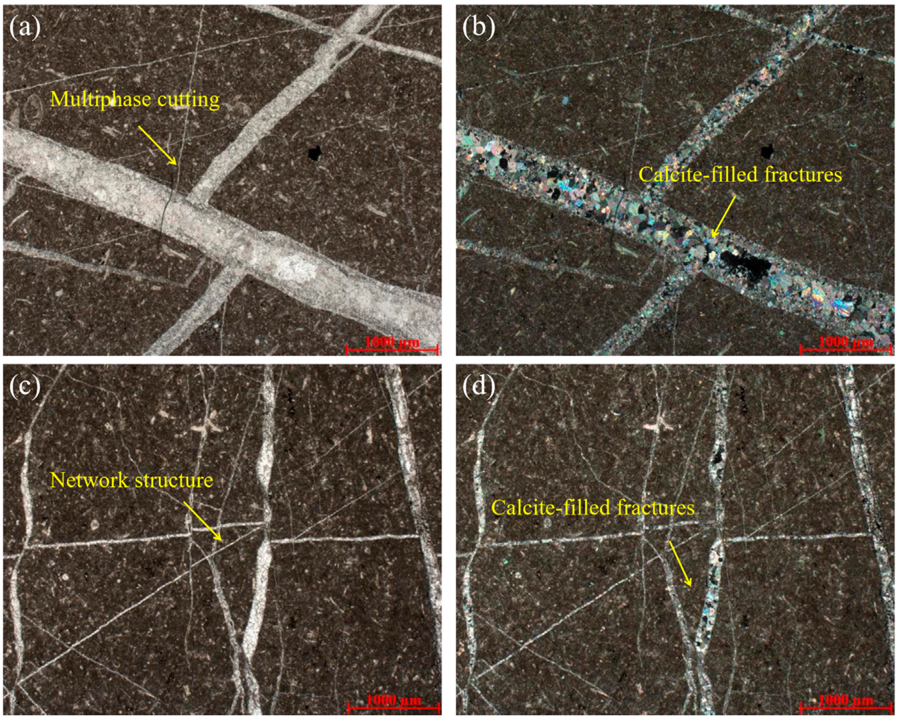

FIGURE 6
Network structure and multiphase cutting features of calcite-filled fractures in the Carboniferous Dawuba Formation shale in well QZY1. **(a, b)** Multiphase cutting in argillaceous limestone, filled with calcite, **(c, d)** Network structure in argillaceous limestone, filled with calcite.

mudstone when subjected to external force. This created numerous gas accumulation sites for shale with poorly developed organic matter pores (Figure 8). These conclusions were also validated by practical work. Well QSD1 achieved good results in vertical well fracturing transformation. Four positions were selected in the "interbedded section," which ultimately yielded a daily industrial gas flow of 11,000 cubic meters of shale gas. During the backflow stage after fracturing, the phenomenon of "rapid gas gathering and rapid back pressure" was observed, which indirectly confirmed the pore characteristics of Lower Carboniferous shale, mainly consisting of micro-fractures and clay mineral interlayer pores. This indicated that shale interbedded with mudstone was conducive to oil and gas retention and pressure sealing. The lithologic interlayer played a positive role in shale gas preservation and was the main gas-bearing layer section.

6 Conclusion

(1) The distinctive reservoir architecture of the Early Carboniferous Dawuba Formation in the Yadu-Ziyun-Luodian Aulacogen (YZLA) originates from its unique Early Carboniferous depositional setting. Located in a platform-basin transitional zone experiencing rapid marine-terrestrial environmental shifts driven by tectonic movements, this dynamic tectonic-sedimentary coupling controlled sediment supply rates. This resulted in the formation of "thin interbedded" sections characterized by frequent vertical stacking of thin-layer mudshales and argillaceous limestones (0.5–5 m single-layer thickness), alongside drastic lateral lithologic variations, establishing the fundamental material-spatial configuration for differential shale gas enrichment.

(2) The Dawuba Formation can be differentiated based on lithologic association and depositional energy. "Interbedded sections," reflecting high-energy deep-water events (like turbidites/storms), feature frequent mudstone-argillaceous limestone interlayering with a mudstone:limestone ratio of 1:1 to 1:2. These sections possess superior reservoir characteristics, including higher average porosity (~2.9%) and higher field desorption gas content (~2.5 m^3/t). They exhibit distinct features like clay mineral seams, dissolution pores, superior pore connectivity, and open micro-fractures, which enhance secondary pore space and permeability. Conversely, "thick-bedded sections," indicative of lower-energy, stable deep-water sedimentation (ratio >1:2), show lower porosity (~2.0%) and lower gas content.

(3) In the tectonically complex YZLA, shale gas content in the Dawuba Formation, particularly the higher content in interbedded sections, is primarily governed by preservation conditions linked to tectonic history and lithologic characteristics, rather than showing clear correlations with TOC abundance, overall porosity, or bulk quartz/clay mineral composition. Favorable preservation in the interbedded sections arises because the mudstone-argillaceous limestone interlayering facilitates the formation of stable micro-fractures, supported by argillaceous limestone layers (gas

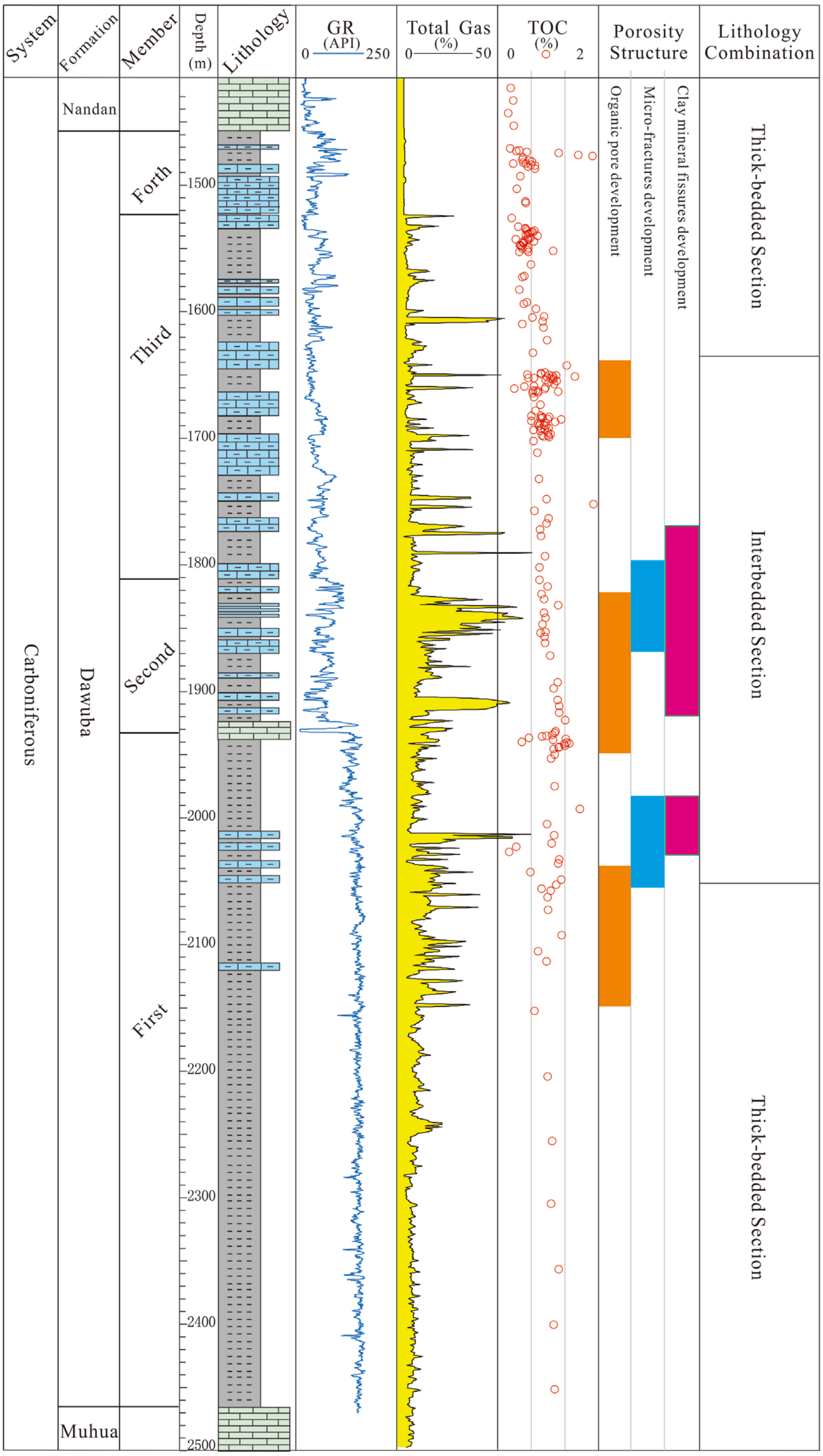

FIGURE 7
Correlation analysis of reservoir characteristics and gas content of Lower Carboniferous shale in well QSD1.

content correlates positively with clay content and mechanical parameters like Poisson's ratio and stresses within these sections) and effectively sealed by the compact argillaceous limestone under stress. This enhances permeability and provides significant storage space for free gas, even where organic matter pores are poorly developed. In contrast, micro-fractures in the more plastic thick-bedded sections tend to close under compaction, reducing storage capacity. Tectonic

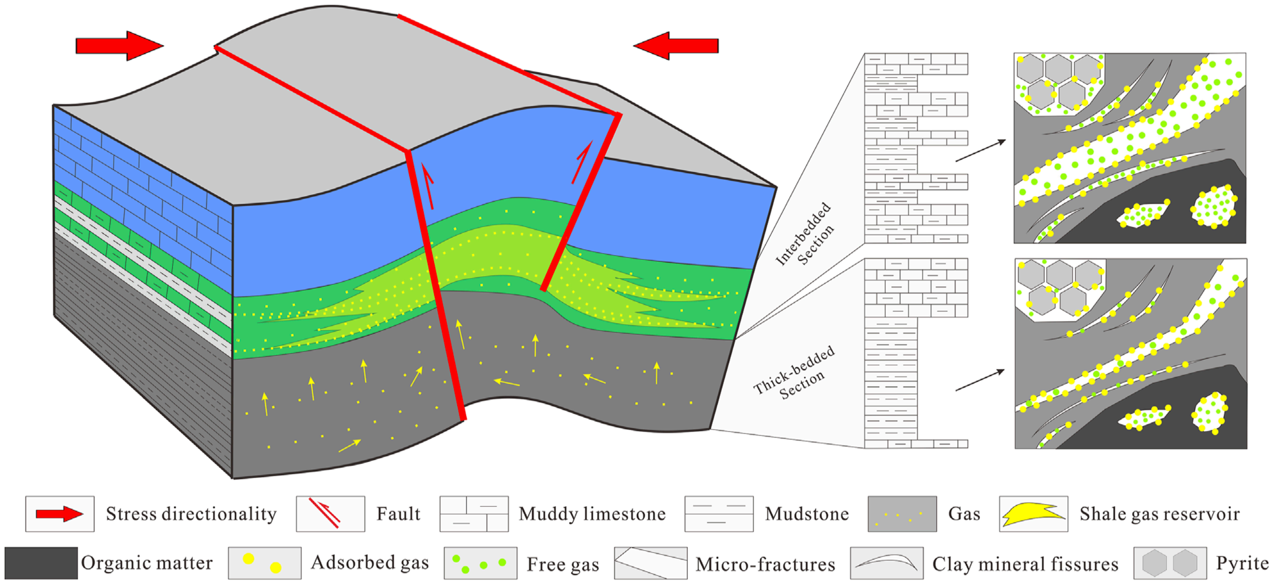

FIGURE 8
Accumulation patterns of shale gas in the Lower Carboniferous shale in southern China (the green part in the left figure represents the interbedded section of mudstone and argillaceous limestone, the gray-black part represents the thick-bedded section).

activity likely altered original gas distributions, diminishing the influence of organic matter adsorption.

(4) The "interbedded sections" of the Early Carboniferous Dawuba Formation are identified as the most favorable intervals for shale gas accumulation and represent the prime exploration targets for achieving shale gas breakthroughs in this Early Carboniferous setting of southern China. These target intervals are characterized by frequent alternations of mudstone and argillaceous limestone with comparable thicknesses (single layers 0.5–5 m, mudstone:limestone ratio 1:1–1:2). Their potential is confirmed by field data (e.g., industrial gas flow in Well QSD1), attributed to the combination of favorable micro-fracture connectivity for storage and the effective pressure-sealing capacity provided by the interbedded lithology, which ensures gas retention.

Data availability statement

The raw data supporting the conclusions of this article will be made available by the authors, without undue reservation.

Author contributions

KY: Conceptualization, Methodology, Validation, Writing – original draft, Writing – review and editing. BF: Investigation, Project administration, Funding acquisition, Writing – original draft. GL: Software, Supervision, Writing – original draft. ZX: Methodology, Validation, Writing – original draft. TL: Data curation, Formal Analysis, Writing – review and editing. XF: Investigation, Validation, Visualization, Writing – review and editing. XS: Data curation, Investigation, Methodology, Writing – review and editing. YX: Methodology, Writing – review and editing. FZ: Resources, Validation, Writing – review and editing.

Funding

The author(s) declare that financial support was received for the research and/or publication of this article. The Guizhou Shale Gas Exploration and Development Co., Ltd. project "Analysis of shale gas resource potential and strategic selection of areas in Guizhou Province" (no. FW2023054) and the Oil and Gas Resources Survey Projects "Investigation and Evaluation of Carboniferous Shale Gas in Southern Guizhou-Central Guangxi" (grant no. ZDDYR2023018) and "Reservoir Characteristics and Gas Accumulation of Trough-platform Shale: A Case Study of Early Carboniferous Shale in Yaziluo Rift Trough" (grant no. YKC2023-YC08).

Acknowledgments

We would like to express our gratitude to Shunshuang Jin, Chao Wang, Xianglin Chen and Peng Gao from Oil and Gas Resources Survey, China Geological Survey for their valuable support and inspiration provided throughout the writing process.

Conflict of interest

Authors BF and GL were employed by the Guizhou Shale Gas Exploration and Development Co., Ltd.

The remaining authors declare that the research was conducted in the absence of any commercial or financial relationships that could be construed as a potential conflict of interest.

Generative AI statement

The author(s) declare that no Generative AI was used in the creation of this manuscript.

Publisher's note

All claims expressed in this article are solely those of the authors and do not necessarily represent those of their affiliated organizations, or those of the publisher, the editors and the reviewers. Any product that may be evaluated in this article, or claim that may be made by its manufacturer, is not guaranteed or endorsed by the publisher.

References

Algeo, T. J., and Lyons, T. W. (2006). Mo-total organic carbon covariation in modern anoxic marine environments: implications for analysis of paleoredox and paleohydrographic conditions. *Paleoceanography* 21, 124–133. doi:10.1029/2004pa001112

Alsaif, M., Becker, M., Donovan, A., and Marcantonio, F. (2024). Investigating the potential of unconventional resources in the Midland Basin: a comprehensive chemostratigraphic analysis of a Cline Shale (Wolfcamp-D) core. *Mar. petroleum Geol.* 168, 107022. doi:10.1016/j.marpetgeo.2024.107022

Arthur, M. A., and Sageman, B. B. (1994). Marine black shales: deposi tional mechanisms and environments of ancient deposits. *Annu. Rev. Earth Pl. Sc.* 22, 499–551. doi:10.1146/annurev.ea.22.050194.002435

Bai, C., Yu, B., Liu, H., Xie, Z., Han, S., Zhang, L., et al. (2018). The genesis and evolution of carbonate minerals in shale oil formations from Dongying depression, Bohai Bay Basin, China. *Int. J. Coal Geol.* 189, 8–26. doi:10.1016/j.coal.2018.02.008

Chabalala, V. P., Wagner, N., Malumbazo, N., and Eble, C. F. (2020). Geochemistry and organic petrology of the permian whitehill formation, Karoo Basin (RSA) and the Devonian/Carboniferous shale of the Appalachian Basin (USA). *Int. J. coal Geol.* 232, 103612. doi:10.1016/j.coal.2020.103612

Chen, H. D., Zhang, J. Q., and Liu, W. J. (1994). Structure of Youjiang basin in Devonian-Carboniferousperiod and its evolution of lithofaciesand palaeogeography. *Guangxi Geol.* 7, 15–23.

Chen, L., Jiang, S., Chen, P., Chen, X., Lu, Y., Zhang, G., et al. (2020). Relative sea-Level changes and organic matter enrichment in the upper ordovician-lower silurian wufeng-longmaxi formations in the central Yangtze area, China. *China. Mar. Petrol. Geol.* 124, 104809. doi:10.1016/j.marpetgeo.2020.104809

Chen, M., Yang, J., Lu, Z., Ming, Y., Wang, H., Chen, S., et al. (2025). Comparison of geological conditions and prospects of exploration potential of shale gas in upper permian Wujiaping formation and Longtan Formation, Sichuan Basin. *Front. Earth Sci.* 13, 1–19. doi:10.3389/feart.2025.1557328

Cheng, G. F., and Xu, A. Q. (1998). An insight into the northwestern-trending tectonical deformation of the Weining-Ziyun belt, western Guizhou. *Guizhou Geol.* 15, 311–320.

Dong, T., Harris, N. B., Ayranci, K., and Yang, S. (2017). The impact of rock composition on geomechanical properties of a shale formation: middle and Upper Devonian Horn River Group shale, Northeast British Columbia, Canada. *AAPG Bull.* 101 (2), 177–204. doi:10.1306/07251615199

Gallego-Torres, D., Martinez-Ruiz, F., Lange, G. J. D., Jimenez-Espejo, F. J., and Ortega-Huertas, M. (2010). Trace-elemental derived paleoceanographic and paleoclimatic conditions for Pleistocene Eastern Mediterranean sapropels. *Palaeogeogr. Palaeoclimatol. Palaeoecol.* 293, 76–89. doi:10.1016/j.palaeo.2010.05.001

Greve, J., Busch, B., Quandt, D., Knaak, M., and Hilgers, C. (2024). Understanding the interplay of depositional rock types, mineralogy, and diagenesis on reservoir properties of the coal-bearing Langsettian and Duckmantian strata (Bashkirian, Pennsylvanian) of the Ruhr Area, NW Germany. *NW Ger.* 113 (8), 2275–2304. doi:10.1007/s00531-024-02454-2

Guo, X., Hu, D., Li, Y., Wei, Z., and Liu, Z. (2017). Geological factors controlling shale gas enrichment and high production in Fuling shale gas field. *Pet. Explor. Dev.* 44, 513–523. doi:10.1016/s1876-3804(17)30060-5

Hao, F., Zou, H., and Lu, Y. (2013). Mechanisms of shale gas storage: implications for shale gas exploration in China. *Aapg. Bull.* 97, 1325–1346. doi:10.1306/02141312091

He, S. J., Li, P. P., Jiang, Z. X., and Tang, X. L. (2025). Multiscale pore structure characteristics of deep marine shale and its control on the gas transport mode. *Phys. fluids* 37. doi:10.1063/5.0251571

Ji, L., Qiu, J., Xia, Y., and Zhang, T. (2012). Micro-pore characteristics and methane adsorption properties of common clay minerals by electron microscope scanning. *Acta Pet. Sin.* 33, 249–256.

Jiang, Y., Dong, D. Z., Qi, L., Shen, Y. F., Jiang, C., and He, F. (2010). Basic features and evaluation of shale gas reservoirs. *Nat. Gas. Ind.* 30, 7–12. doi:10.3787/j.issn.1000-0976.2010.10.002

Jones, B., and Manning, D. A. (1994). Comparison of geochemical indicesused for the interpretation of palaeoredox conditions in ancientmudstones. *Chem. Geol.* 111, 111–129. doi:10.1016/0009-2541(94)90085-x

Khan, N., Littke, R., Weltje, G. J., and Swennen, R. (2024). Black shale deposition during the Paleocene–Eocene thermal maximum: shale-gas potential of the Patala Formation, Himalayan fold-and-thrust belt, Pakistan (eastern Tethys). *Pak. East.(Tethys)* 113, 2189–2205. doi:10.1007/s00531-024-02436-4

Li, X., Lu, S. F., Zhang, X. G., Zhao, S. X., Yang, X. F., Liu, Y. Y., et al. (2025). Deep shale gas-bearing parameters evaluation method based on carbon isotope fractionation and logging data. *Energy fuels.* 39, 1152–1165. doi:10.1021/acs.energyfuels.4c05104

Li, X., Wang, Y., Lin, W., Ma, L., Liu, D., and Zhang, Y. (2022a). Tectonic characteristics and its effect on shale gas preservation condition in the jingmen region. *Front. Earth Sci.* 9, 1–23. doi:10.3389/feart.2021.821593

Li, X. F., Yuan, K., Fang, X. X., and Wang, T. (2022b). Carbon and oxygen isotope composition of carbonate minerals in carbonaceous shale and its geological significance—a case study from the Carboniferous Dawuba Formation shale, southern Guizhou area China. *Fresenius Environ. Bull.* 31, 990–997.

Li, Y., Shao, D., Lv, H., Zhang, Y., and Zhang, T. (2015). A relationship between elemental geochemical characteristics and organic matter enrichment in marine shale of Wufeng Formation-Longmaxi Formation, Sichuan Basin. *Acta Pet. Sin.* 36, 1470–1483. doi:10.7623/syxb201512002

Liu, G., Huang, Z., Jiang, Z., Chen, J., Chen, F., and Xing, J. (2016). Gas adsorption capacity calculation limitation due to methane adsorption in low thermal maturity shale: a case study from the Yanchang Formation, Ordos Basin. *J. Nat. Gas. Sci. Eng.* 30, 106–118. doi:10.1016/j.jngse.2016.01.026

Liu, J. P., Ma, J., and Wang, X. W. (2006). Characteristics of the segments of the Ziyun deformation belt in the Nanpanjiang area, Guizhou, China. *J. Chengdu Univ. Technol.* 33, 15–18.

Liu, W. H., Tenger, B., Wang, X. F., Li, M. W., Hu, G., Wang, J., et al. (2017). New knowledge of hydrocarbon generating theory of organic matter in Chinese marine carbonates. *Pet. Explor. Dev.* 41, 155–164. doi:10.1016/S1876-3804(17)30020-4

Loucks, R. G., Reed, R. M., Ruppel, S. C., and Hammes, U. (2012). Spectrum of pore types and networks in mudrocks and a descriptive classification for matrix-related mudrock pores. *AAPG Bull.* 96, 1071–1098. doi:10.1306/08171111061

Ma, K., Pang, H., Zhang, L., Huang, S., Huo, X., and Chen, J. (2022a). Hydrocarbon dynamic field division and its relevance to oil and gas exploration for Paleogene reservoir in Lufeng Depression. *Adv. Geo-Energy Res.* 6, 415–425. doi:10.46690/ager.2022.05.06

Ma, X., Wang, H., Zhou, T., Zhao, Q., Shi, Z., Sun, S., et al. (2022b). Geological controlling factors of low resistivity shale and their implications on reservoir quality: a case study in the southern Sichuan Basin, China. *Energies* 15, 5801. doi:10.3390/en15165801

Ma, Y. S., He, D. F., Cai, X. Y., and Liu, B. (2017). Distribution and fundamental science questions for petroleum geology of marine carbonate in China. *Acta Petrol. Sin.* 33, 1007–1020.

Mansour, A., Wagreich, M., Tahoun, S. S., Ahmed, M. S., and Gentzis, T. (2024). Paleoredox conditions, paleoproductivity, and terrigenous sediment influx of the lower-middle cenomanian strata in the abu gharadig basin, northern Egypt. *Minerals* 14, 632. doi:10.3390/min14060632

Martyushev, D. A., Ponomareva, I. N., Chukhlov, A. S., Davoodi, S., Osovetsky, B. M., Kazymov, K. P., et al. (2023). Study of void space structure and its influence on carbonate reservoir properties: X-ray microtomography, electron microscopy, and well testing. *Geol.* 151, 106192. doi:10.1016/j.marpetgeo.2023.106192

Mcmahon, T. P., Larson, T. E., Zhang, T., Shuster, M., Mcmahon, T., and Larson, T. (2024). Geologic characteristics,exploration and production progress of shale oil and gas in the United States:An overview. *Petroleum Explor. Dev.* 51, 925–948. doi:10.1016/s1876-3804(24)60516-1

Milliken, K. L., Rudnicki, M., Awwiller, D. N., and Zhang, T. (2013). Organic matter-hosted pore system, marcellus formation (Devonian), Pennsylvania. *AAPG Bull.* 97, 177–200. doi:10.1306/07231212048

Nie, H. K., Tang, X., and Bian, R. K. (2009). Controlling factors for shale gas accumulation and prediction of potential development area in shale gas reservoir of South China. *Acta Pet. Sin.* 30, 484–491. doi:10.7623/syxb200904002

Peng, J., Chen, H. D., Tian, J. C., Qin, J. X., Hou, Z. J., Yang, X. N., et al. (2000). Sequence stratigraphy study on the cabroniferous strata in sichuan, yunnan, Guizhou and Guangxi. *Acta Sedimentol. Sin.* 18, 190–197.

Rezaeyan, A., Kampman, N., Pipich, V., Barnsley, L. C., Rother, G., Magill, C., et al. (2023). Evolution of pore structure in organic-lean and organic-rich mudrocks. *Energy and Fuels* 37 (21), 16446–16460. doi:10.1021/acs.energyfuels.3c02180

Sageman, B. B., Murphy, A. E., Werne, J. P., Straeten, C. A. V., and Lyons, T. W. (2003). A tale of shales: the relative roles of production, decomposition, and dilution in the accumulation of organic-rich strata, Middle–Upper Devonian, Appalachian basin. *Chem. Geol.* 195, 229–273. doi:10.1016/s0009-2541(02)00397-2

Scott, L. M., Daniel, M. J., Kent, A. B., and Pollastro, R. M. (2005). Mississippian Barnett shale, Fort Worth Basin, north-central Texas: gas-shale play with multitrillion cubic foot potential. *AAPG Bull.* 89, 155–175. doi:10.1306/09170404042

Srinivasan, S., O'Malley, D., Mudunuru, M. K., Sweeney, M. R., Hyman, J. D., Karra, S., et al. (2021). A machine learning framework for rapid forecasting and history matching in unconventional reservoirs. *Sci. Rep.* 11, 21730. doi:10.1038/s41598-021-01023-w

Valdon, Y. B., Oboh-Ikuenobe, F. E., Maigari, S. A., and Zobaa, M. K. (2023). Source-rock potential and paleoenvironment of the Coniacian Numanha Formation, northeastern Nigeria: an integrated palynofacies and geochemical approach. *J. Afr. earth Sci.* 198, 104790. doi:10.1016/j.jafrearsci.2022.104790

Wang, K., Yang, H., Li, Y., Zhang, R., Ma, Y., Wang, B., et al. (2021). Geological characteristics and exploration potential of the northern tectonic belt of Kuqa depression in Tarim Basin. *Acta Pet. Sin.* 42, 885–905. doi:10.7623/syxb202107005

Wang, S. Y. (2016). Faults and earthquakes in Guizhou. *J. Geomech.* 22, 430–438. doi:10.3969/j.issn.1006-6616.2016.03.004

Wang, T., Xu, Z., Yuan, K., Wang, X., and Ge, M. (2024). Paleoenvironment and shale gas potential of the carboniferous Dawuba and the cambrian Niutitang shales in the upper Yangtze platform, south China. *Front. Earth Sci.* 12, 1404178. doi:10.3389/feart.2024.1404178

Wang, Y., Xu, S., Hao, F., Lu, Y., Shu, Z., Detian, Y., et al. (2018). Geochemical and petrographic characteristics of Wufeng-Longmaxi shales, Jiaoshiba area, southwest China: implications for organic matter differential accumulation. *Mar. Petrol. Geol.* 102, 138–154. doi:10.1016/j.marpetgeo.2018.12.038

Xia, W. C., Zhou, J., Lei, J. X., Zhang, N. M., and Peng, Y. (1995). The evolution of the rifted oceanic basin due to lithosperic stretching in Yunnan-Guizhou and Guangxi provinces during the late Hercynian to middle Indosinian stage. *Acta Geol. Sin.* 69, 97–112.

Yang, Q., Mao, Z., and Shao, M. R. (2021). Research methods and prospects of nanopore structure in shale gas reservoirs. *Energy Chem. Ind.* 42, 7–13. doi:10.3969/j.issn.1006-7906.2021.02.003

Yang, Y. R., Liu, X. C., Zhang, H., Zhai, G. Y., Zhang, J. D., Hu, Z. F., et al. (2019). A review and research on comprehensive characterization of microscopic shale gas reservoir space. *China Geol.* 2, 541–556. doi:10.31035/cg2018116

Yuan, K., Chen, R., Lin, T., Fang, X., Qin, Y., and Wang, C. (2019). Petrological characteristics and sedimentary environment in the southern Guizhou during the Late Carboniferous. *Pet. Geol. Exp.* 41, 38–44. doi:10.11781/sysydz201901038

Yuan, K., Fang, X. X., Lin, T., Bao, S. J., Shi, D. S., and Zhang, C. (2017). Geochemical features and sedimentary conditions of Middle-Devonian shale in the northwestern central Guangxi depression. *Geol. Explor* 53, 179–186.

Yuan, K., Huang, W. H., Chen, X. L., Cao, Q., Fang, X. X., Lin, T., et al. (2022). The whole-aperture pore structure characteristics and their controlling factors of the Dawuba Formation shale in Western Guizhou. *Processes* 10, 622. doi:10.3390/pr10040622

Yuan, K., Wang, C., Qin, Y., Yu, S., Chen, R., Shi, D., et al. (2017). The discovery of Carboniferous shale gas in Qianziye-1 well of Qianan (southern Guizhou) depression. *Geol. China* 44, 1253–1254. doi:10.12029/gc20170615

Yuan, K., Wang, K., Gong, S., Lu, S., and Fang, X. (2018). Shale gas enrichment features and impacting factors in carboniferous Dawuba Formation, southern Guizhou area. *Coal Geol. China.* 30, 28–34. doi:10.3969/j.issn.1674-1803.2018.03.05

Zeng, Y. F., Liu, W. J., Chen, H. D., Zheng, R. C., Zhang, J. Q., Li, X. Q., et al. (1992). The sedimentary characteristics and structural evolution of the Youjiang composite basin. *Guangxi Geol.* 5, 1–14.

Zheng, F. Z., Yuan, K., Shan, J. F., Lin, T., You, M. X., Niu, J. L., et al. (2022). Evaluation of shale gas content and preservation conditions in complex structural areas: a case study of Dawuba Formation of the Yaziluo fault zone in southwest Guizhou province. *China Offshore Oil Gas* 34 (4), 109–121. doi:10.11935/j.issn.1673-1506.2022.04.010

Zou, C., Qiu, Z., Poulton, S. W., Dong, D., Wang, H., Chen, D., et al. (2018). Ocean euxinia and climate change "double whammy" drove the Late Ordovician mass extinction. *Geology* 46, 535–538. doi:10.1130/g40121.1

Zou, C., Zhu, R., Chen, Z., Ogg, J. G., Yang, Z., Dong, D., et al. (2019). Organic-matter-rich shales of China. *Earth-Sci. Rev.* 189, 51–78. doi:10.1016/j.earscirev.2018.12.002